



## Aerodynamic analysis of different cyclist hill descent positions

Bert Blocken <sup>a,b,\*</sup>, Thijs van Druenen <sup>a</sup>, Yasin Toparlar <sup>a</sup>, Thomas Andrianne <sup>c</sup>

<sup>a</sup> Department of the Built Environment, Eindhoven University of Technology, P.O. Box 513, 5600, Eindhoven, the Netherlands

<sup>b</sup> Department of Civil Engineering, KU Leuven, Kasteelpark Arenberg 40 – Bus 2447, 3001, Leuven, Belgium

<sup>c</sup> Department of Aerospace and Mechanical Engineering, University of Liège, Allée de la Découverte, 9 Quartier Polytech 1, B52/3, B-4000, Liège, Belgium

### ARTICLE INFO

#### Keywords:

Cycling position  
Computational fluid dynamics  
Numerical simulation  
Wind tunnel  
Aerodynamic cyclist drag  
Cycling aerodynamics

### ABSTRACT

Different professional cyclists use very different hill descent positions, which indicates that prior to the present study, there was no consensus on which position is really superior, and that most cyclists did not test different positions, for example in wind tunnels, to find which position would give them the largest advantage. This paper presents an aerodynamic analysis of 15 different hill descent positions. It is assumed that the hill slope is steep enough so pedaling is not required to gain speed and that the descent does not include sharp bends necessitating changes in position. The analysis is performed by Computational Fluid Dynamics (CFD) simulations with the 3D RANS equations and the Transition SST  $k-\omega$  model. The simulations are validated wind tunnel measurements. The results are analyzed in terms of frontal area, drag area and surface pressure coefficient. It is shown that the infamous “Froome” position during the Peyresourde descent of Stage 8 of the 2016 Tour de France is not aerodynamically superior to several other positions. Other positions are up to 7.2% faster and also safer because they provide more equal distribution of body weight over both wheels. Also several positions that allow larger power generation are aerodynamically superior.

### 1. Introduction

It is well-known that the greatest potential for improvement in cycling speed is situated in its aerodynamics (Wilson, 2004). At racing speeds (about 54 km/h or 15 m/s), the aerodynamic resistance or drag is about 90% of the total resistance (Kyle and Burke, 1984; Grappe et al., 1997; Lukes et al., 2005). In hill descents however, higher speeds can be achieved, up to 110 km/h and beyond (Vanmarcke, 2017). To gain as much speed as possible in hill descents, different professional cyclists adopt very different positions, as shown in Fig. 1. This indicates that, at least prior to this research, which was first announced by means of a Linked In article on 28 April 2017, there was no consensus on which position is aerodynamically superior, and that most cyclists did not test different positions, for example in wind tunnels, to find which position would give them the largest advantage.

This study was incited by the specific hill descent position assumed by professional cyclist Chris Froome in stage 8 of the 2016 Tour de France. Fig. 2a shows the altitude profile and Fig. 2b the map of this stage. The stage ended with the descent of the Peyresourde. As shown in Fig. 2, the descent of the Peyresourde is steep and not characterized by sharp bends. At the day of the descent, the weather conditions were good and the road

surface was dry. Near the very end of this stage, just before the top of the Peyresourde, cyclist Chris Froome accelerated and broke away from the group. During part of the hill descent, he adopted the position shown in Fig. 1a and achieved speeds up to 90 kmh. Finally, he won the stage and took the prestigious yellow jersey. The question arises to what extent this particular descent position provides aerodynamic benefits that are not provided by other, more commonly adopted hill descent positions.

Aerodynamic drag in cycling can be assessed by field tests, wind tunnel measurements and numerical simulation by Computational Fluid Dynamics (CFD) (Blocken, 2014; Crouch et al., 2017). Previous aerodynamic studies in cycling have focused on cyclists in different types of race or time trial positions, either isolated or followed by other cyclists, motorcycles or cars (e.g. Kyle and Burke, 1984; Dal Monte et al., 1987; Zdravkovich et al., 1996; Grappe et al., 1997; Padilla et al., 2000; Jeukendrup and Martin, 2001; Hanna, 2002; Lukes et al., 2004; Defraeye et al., 2010a, 2010b; 2011, 2014; Blocken et al., 2013, 2016; Crouch et al., 2014; Griffith et al., 2014; Blocken and Toparlar, 2015; Fintelman et al., 2014a, 2015a; Barry et al., 2015; Beaumont et al., 2018). Recent studies have also focused on Paralympic tandem cycling (Mannion et al., 2018a, 2018b), Paralympic handcycling (Mannion et al., 2018c) and even on full cyclist pelotons (Blocken et al., 2018). However, to the best

\* Corresponding author. Department of the Built Environment, Eindhoven University of Technology, P.O. Box 513, 5600 MB Eindhoven, the Netherlands.  
E-mail address: [b.j.e.blocken@tue.nl](mailto:b.j.e.blocken@tue.nl) (B. Blocken).

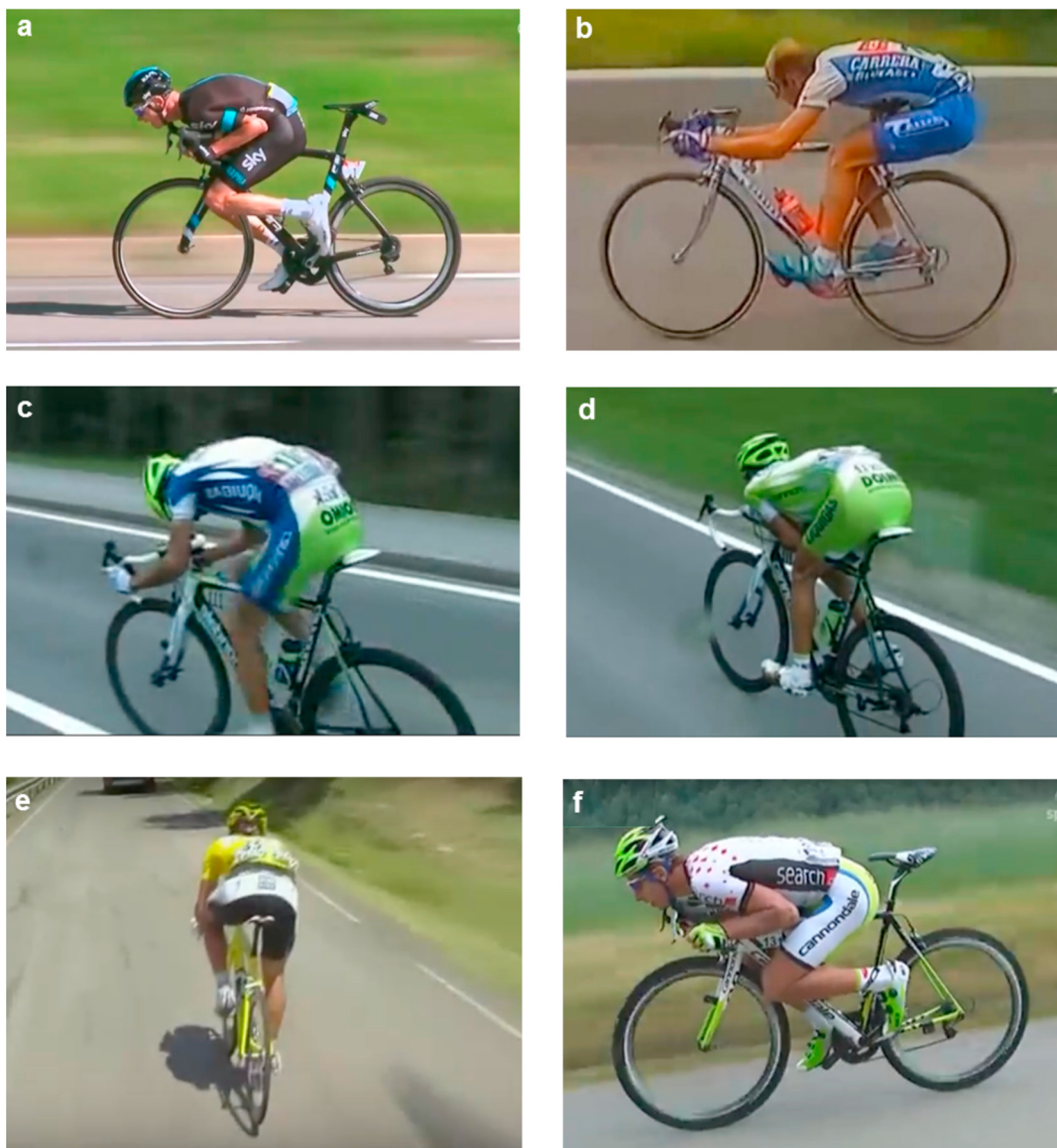


**Fig. 1.** Hill descent positions as adopted by professional cyclists: (a) Chris Froome on front part of top tube; (b) Marco Pantani behind saddle; (c) Vincenzo Nibali on saddle in “back horizontal” position; (d) Vincenzo Nibali with forearms tucked in (“puppy paws” position); (e) Fabian Cancellara in “back up” position; (f) Peter Sagan on rear part of top tube. Source: VRT/Sporza.

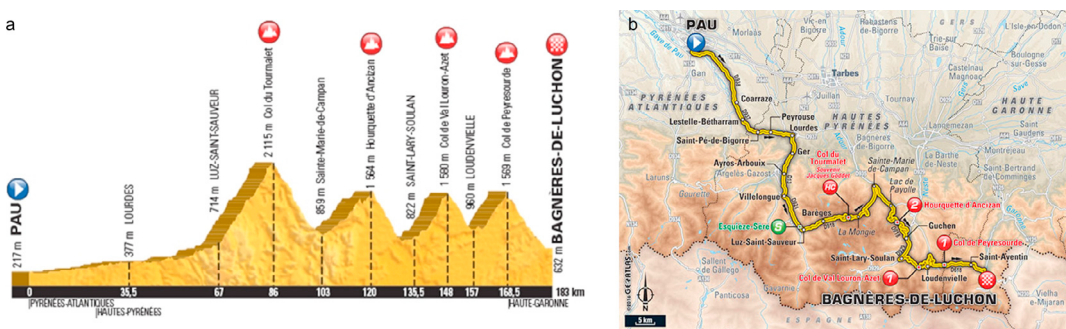


**Fig. 2.** Stage 8 of the Tour de France 2016. (a) Altitude profile and (b) Map of stage. Source: touretappe.nl.

of our knowledge, no previous study focused on specific hill descent positions.

This paper therefore provides an aerodynamic analysis of different hill descent positions. Evidently, in most professional descents, the aerodynamic performance of a given position is not the sole criterion,

also the ability to provide power by pedaling (see Grappe et al., 1998; Fintelman et al., 2014b, 2015b; 2016) and steering capability in sharp bends are important. However, in the present paper, we focus on steep descents without many sharp bends, similar to the Peyresourde descent in the 2016 Tour de France.

The paper is structured as follows. Section 2 reports the set-up of the wind tunnel experiments. Section 3 presents the CFD simulations for the validation study. Section 4 presents the results of the CFD simulations for 15 different cyclist positions. Finally, sections 5 (discussion) and 6 (conclusions) conclude the paper.

## 2. Wind tunnel measurements

Four cyclist positions were selected for the wind tunnel measurements (Fig. 3). The cyclist geometry was obtained by scanning a cyclist in different positions using an Eva structured 3D light scanner (Artec Europe, 2017). The same cyclist was used for all positions to remove anthropometric bias. Written consent of the scanned athlete was obtained. The athlete had a height of 1.83 m and a weight of 72 kg. Side views of these four positions together with the seven characteristic angles specifying the position on the bicycle are given in Fig. 3. The legs of the cyclist were static and both wheels of the bicycle were fixed. The bicycle geometry was simplified, specifically concerning the front forks, wheel hubs and spokes, pedals, cranks and handlebars. Some elements of the bicycle were neglected as they were considered small enough not to influence the characteristic flow around it. These included the chains, sprockets and also brake and gear cables and mechanisms. The full-scale frontal areas (including bicycle) were 0.344 m<sup>2</sup> for the “Froome” position, 0.343 m<sup>2</sup> for the “Pantani” position, 0.370 m<sup>2</sup> for the “Back horizontal” position and 0.339 m<sup>2</sup> for the “Back down 1” position.

The wind tunnel measurements were performed in the aeronautical section of the wind tunnel at the University of Liège in Belgium. The cross-section of the test section is W x H = 2 × 1.5 m<sup>2</sup>. A dedicated set-up with an elevated sharp-edge horizontal plate and embedded force balance was developed by the technical staff at Eindhoven University of Technology and installed in the Liège wind tunnel to limit boundary layer

development (Fig. 4). To fully accommodate the models in the wind tunnel at a blockage ratio below 5%, they were manufactured at scale ¼, yielding a blockage ratio below 3.5%. Fig. 5 shows the models in the wind tunnel. Tests were performed at 60 m/s to ensure Reynolds number similarity with the (full-scale) CFD simulations and with reality at 15 m/s cycling speed. Drag in cycling is often quantified by the drag area  $A_{CD}$  (m<sup>2</sup>), which is the product of the frontal area of the cyclist and bicycle (A) and the drag coefficient ( $C_D$ ). It relates the drag force ( $F_D$ ) to the dynamic pressure ( $\rho U_\infty^2/2$ ):

$$F_D = A_{CD} \frac{\rho U_\infty^2}{2} \quad (1)$$

where  $\rho$  is the density of air (kg/m<sup>3</sup>) and  $U_\infty$  the approach-flow air speed (m/s). The drag force, i.e. the horizontal component parallel to the wind direction and bicycle, was measured using a force transducer with a conservative maximum error estimate of 1.24 N with 95% confidence level, although the actual precision is expected to be much better (Gore, 2016). Note that this error includes both systematic and random errors, and that systematic errors were removed by biasing prior to every measurement. The data were sampled at 10 Hz for 180 s. During the measurements, air temperature, speed and atmospheric pressure were recorded to correct the measurements to the references values of 15 °C, 15 m/s and 101325 Pa as in the CFD simulations. The measurements were also corrected by subtracting the drag of the base plate (see Fig. 5) as well as for blockage using the expressions for solid blockage reported by Barlow et al. (1999). The boundary-layer height was 6 cm, which was below the feet and pedals of the cyclist. The longitudinal turbulence intensity of the approach flow was lower than 0.2%.

The measurement results in terms of drag area are given in Fig. 6 and demonstrate that the “Pantani” position has the lowest drag area

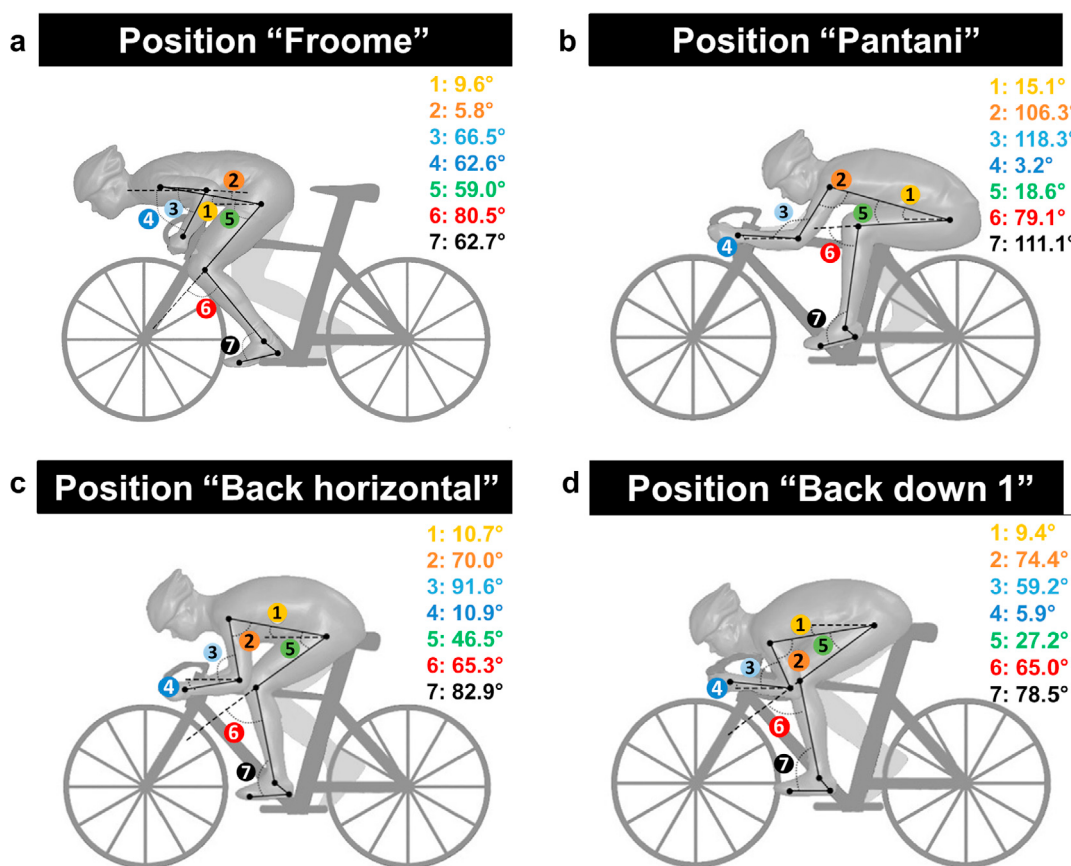


**Fig. 3.** The four cyclist positions with definition and values of (1) sagittal torso angle; (2) shoulder angle; (3) elbow angle; (4) forearm angle; (5) hip angle; (6) knee angle; (7) ankle angle.

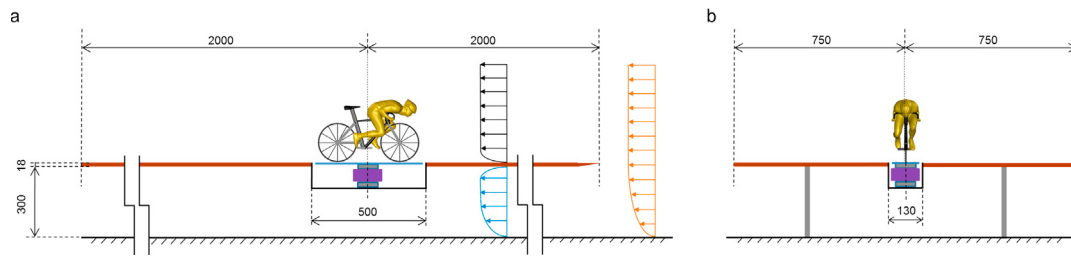


**Fig. 4.** Wind tunnel set-up with model on elevated sharp-edged plate to reduce boundary-layer thickness. Dimensions in mm.

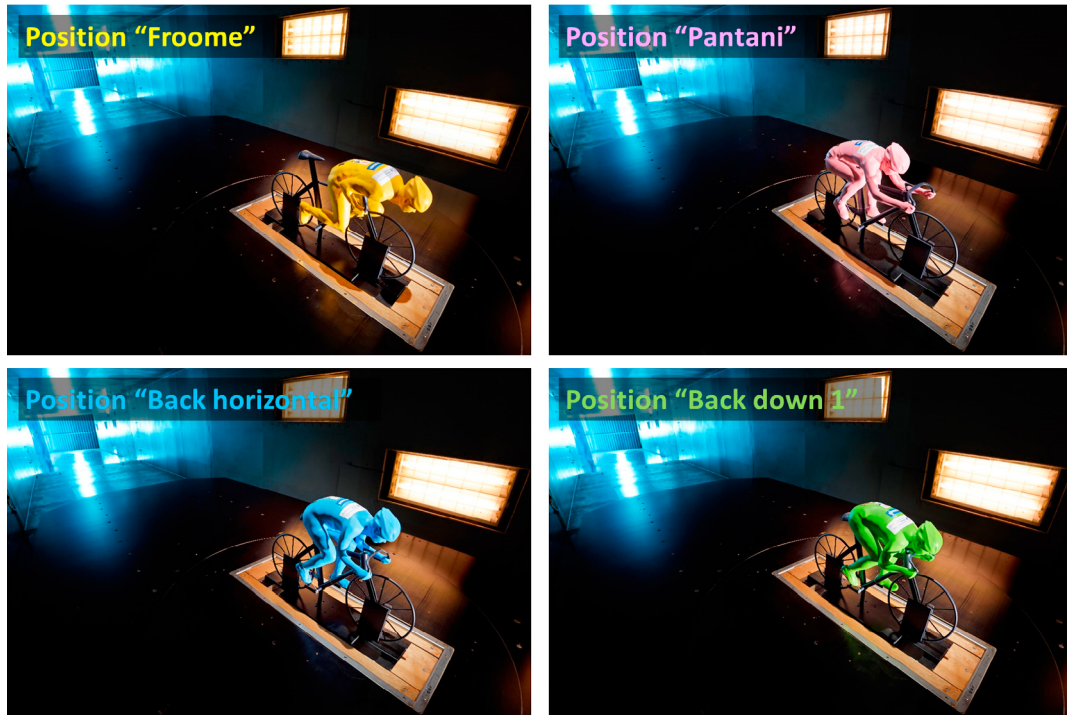


**Fig. 5.** Quarter-scale models in the wind tunnel.

( $0.228 \text{ m}^2$ ), followed by the position "Back down 1" ( $0.239 \text{ m}^2$ ) and the "Froome" position ( $0.258 \text{ m}^2$ ). Finally, the "Back horizontal" position ( $0.272 \text{ m}^2$ ) has the highest drag area of the four positions tested.

### 3. CFD simulations – part I: validation

#### 3.1. Computational geometry and domain

CFD simulations were performed for the four positions tested in the wind tunnel. The simulations were performed at full scale. The models were placed in a computational domain with size according to best practice guidelines (Franke et al., 2007; Tominaga et al., 2008; Blocken, 2015) (Fig. 7). The size of the computational domain was  $L \times W \times H = 33.79 \times 16.49 \times 9.73 \text{ m}^3$ . The maximum blockage ratio was 0.2%, which is well below the recommended maximum value of 3% (Franke et al., 2007; Tominaga et al., 2008). The directional blockage ratios were also well below 17% (Blocken, 2015). Given these low blockage ratios, the CFD simulations were not corrected for blockage.

#### 3.2. Computational grid

The grids were based on grid sensitivity analysis and grid generation guidelines in CFD (Casey and Wintergerste, 2000; Tucker and Mosquera, 2001; Franke et al., 2007; Tominaga et al., 2008). The grid sensitivity

analysis indicated the requirement for a wall-adjacent cell size of 20 micrometer at the cyclist and bicycle surfaces and a prismatic boundary layer mesh of 40 layers of incremental thickness with a maximum growth ratio of 1.1. The small wall-adjacent cell size and the 40 layers were important to fully resolve the thin viscous/laminar sublayer and the buffer layer, which was important to correctly reproduce boundary layer separation, reattachment and laminar-to-turbulent transition. The dimensionless wall unit  $y^*$  was generally lower than 1, although very locally a maximum value of 5 was reached. Outside the 40 layers, tetrahedral and/or prismatic cells were used. The grids for the four positions are shown in Fig. 8. Fig. 9 shows details of the computational grid, including the near-wall grid layers at the cyclist and bicycle surface.

#### 3.3. Boundary conditions

At the inlet, a uniform velocity of 15 m/s was imposed with a turbulence intensity of 0.2%, representing the relative air movement due to cycling at this speed in still air (zero wind speed). The cyclist and bicycle surfaces were modeled as smooth no-slip walls corresponding to the smooth surface finish of the wind tunnel models. For the bottom boundary of the domain, a slip wall was defined. For the side and top boundaries of the domain, symmetry conditions were imposed. At the outlet, zero static gauge pressure was imposed.

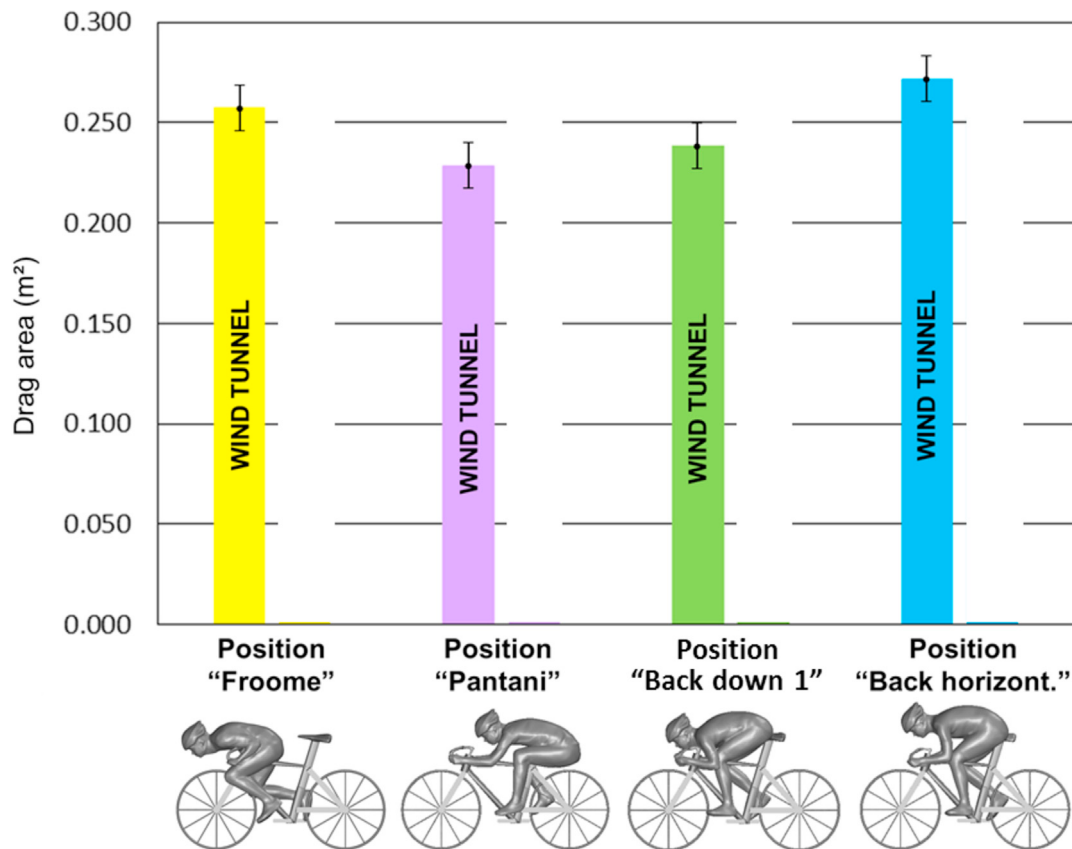


**Fig. 6.** Wind tunnel results for the four tested models in terms of drag area.

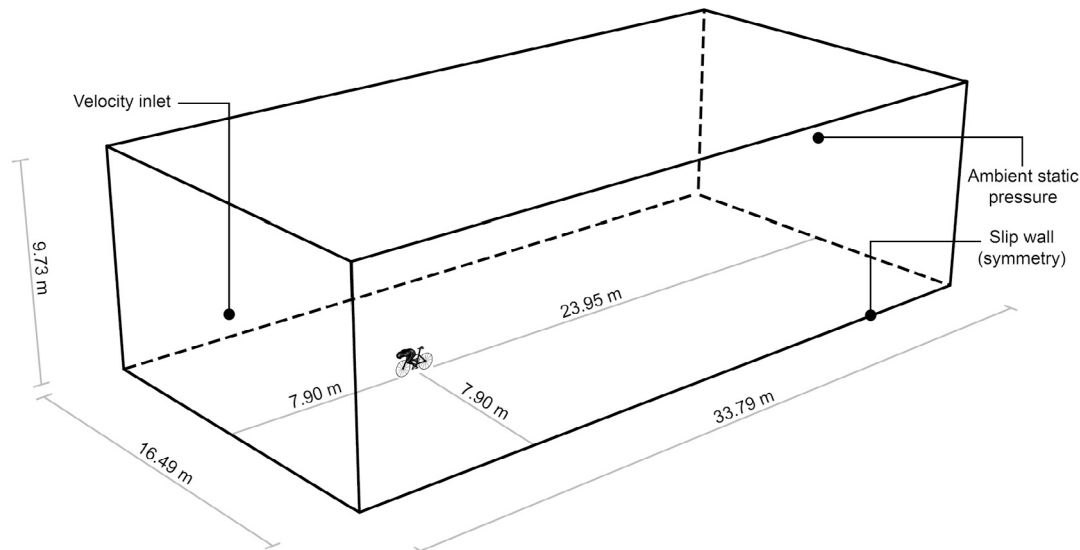


**Fig. 7.** Computational domain with main dimensions and main boundary conditions.

### 3.4. Approximate form of governing equations and solver settings

The 3D RANS equations were solved with the Langtry-Menter 4-equation Transition Shear Stress Transport (SST)  $k-\omega$  model (Menter et al., 2006; Langtry and Menter, 2009). This turbulence model, also known as the  $\gamma$ - $Re_\theta$  model, is implemented in ANSYS 15 and 16 (ANSYS, 2013) and is based on the coupling of the SST  $k-\omega$  transport equations with two

additional transport equations, one for the intermittency and one for the transition onset criteria, in terms of momentum thickness and Reynolds number. The model was applied here with inclusion of curvature correction and with production limiters (ANSYS, 2013). Pressure-velocity coupling was taken care of with the coupled scheme, pressure interpolation was second order and second-order discretization schemes were used for both the convection terms and the viscous terms of

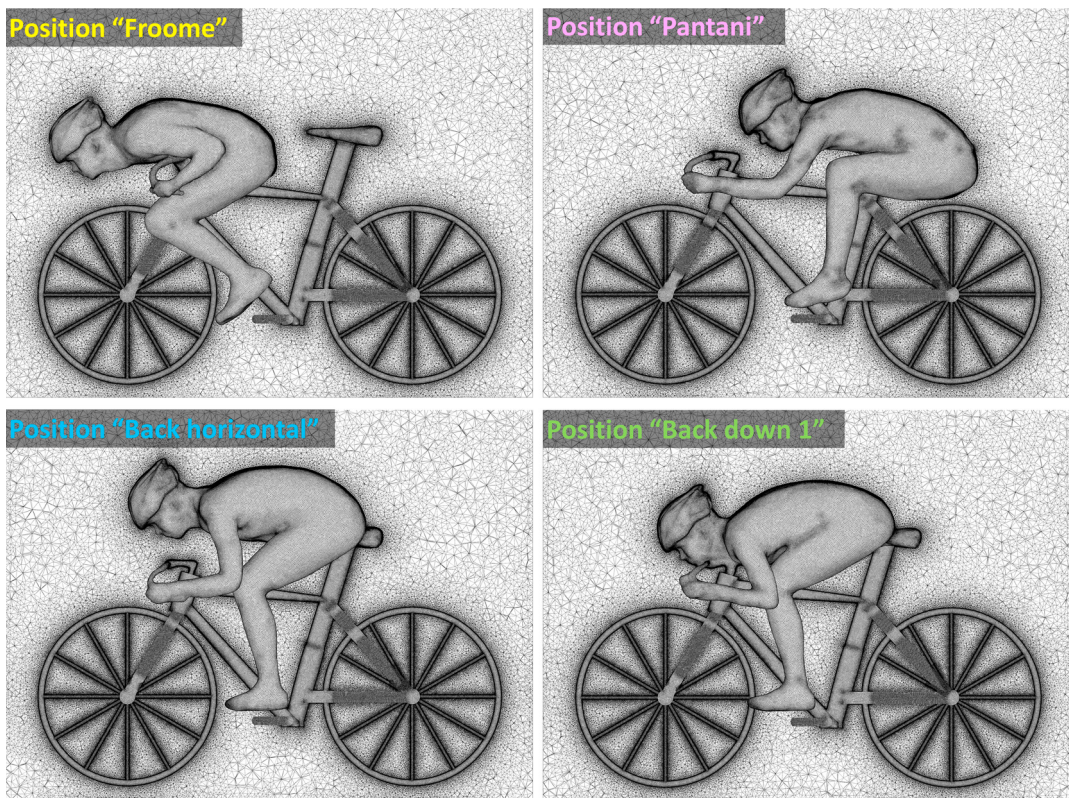


**Fig. 8.** Computational grids for the four positions on the cyclist and bicycle surfaces and in the vertical centerplane. Total cell counts: (a) 36,404,649; (b) 38,885,578; (c) 37,744,105; (d) 37,748,609.

the governing equations. Second order was also applied for the four turbulence model equations. The gradients were computed with the Green-Gauss cell-based method (ANSYS, 2013). The simulations were performed with the commercial CFD code ANSYS Fluent, release 16. The pseudo-transient under-relaxation method was employed with 6000 time steps of 0.01 s. Results were obtained by averaging over the last 5000 pseudo-transient time steps.

### 3.5. Results

**Fig. 10** compares the drag areas obtained by CFD with those by the wind tunnel measurements. The CFD simulations provided the same trends as the wind tunnel measurements: the lowest drag area for the “Pantani” position, followed by the “Back down 1” position and the “Froome” position, and finally the “Back horizontal” position. The deviations between the CFD results and the wind tunnel results were 3.1%, 0.1%, 2.2% and 7.2% for the “Froome”, “Pantani”, “Back down 1” and “Back horizontal” position, respectively. The reason for the less good agreement for the latter position is not totally clear. It is possible that the separation points/lines on the surface of this particular model are located at positions where the resulting drag is more sensitive to a small shift in these positions, and hence more difficult to reproduce computationally. However, given the overall close agreement, the same computational parameters and settings were used for the parametric study in the next section. Note that the CFD simulations were performed for an approach-flow wind speed of 15 m/s and that the wind tunnel measurements were performed for an approach-flow wind speed at 60 m/s at reduced scale (quarter scale), corresponding to 15 m/s at full scale. Hill descent speeds however will generally be significantly higher. CFD simulations for the four different cyclist positions were also performed for 20 m/s (72 km/h) and 25 m/s (90 km/h) which yielded nearly the same drag areas for every position (deviations below 0.5%).

## 4. CFD simulations – part II: parametric analysis

### 4.1. Computational geometry

CFD simulations were performed for fifteen different positions, i.e. the four positions from the validation study and eleven additional positions. The same cyclist was scanned for the eleven additional positions to remove anthropometric bias. **Fig. 11** displays the five selected positions where the cyclists are sitting on the saddle together with the associated frontal areas: (a) the regular “Back up” position; (b) the “Back horizontal” position; (c) the “Back down 1” position with hands on the drops; (d) the “Back down 2” position with hands close to each other on top of the handlebar, in the field sometimes referred to as “position puppy paws”; and (e) the “Elbows” position with the elbows resting on top of the handlebar and the hands detached from and in front of the handlebar. **Fig. 12** shows the five selected positions where the cyclists are sitting on the top tube, together with the frontal areas: (a) the “Froome” position, where the athlete is sitting on the front part of the top tube with the torso bent over the handlebar; (b) the “Top tube 1” position, where the cyclist is sitting more towards the rear of the top tube, with the torso fairly upright; (c) the “Top tube 2” positions, with the cyclist sitting at the very rear of the top tube but with torso fairly upright, although less than in **Fig. 12b**; (d) the “Top tube 3” position, with the cyclist at the very rear of the top tube and with the torso as horizontal as possible; and (e) the “Top tube 4” position, which is identical to the “Top tube 3” position but with the head tilted further down. **Fig. 13** illustrates the five remaining positions and their frontal areas: (a) the “Pantani” position; (b) the regular time trial position with time trial helmet; (c) the top tube time trial position with time trial helmet; (d) the time trial position with regular helmet; and (e) a stunt position called the “Superman” position, which is not an allowed race position but which was included here for completeness as it had been used by a stunt man to show superior

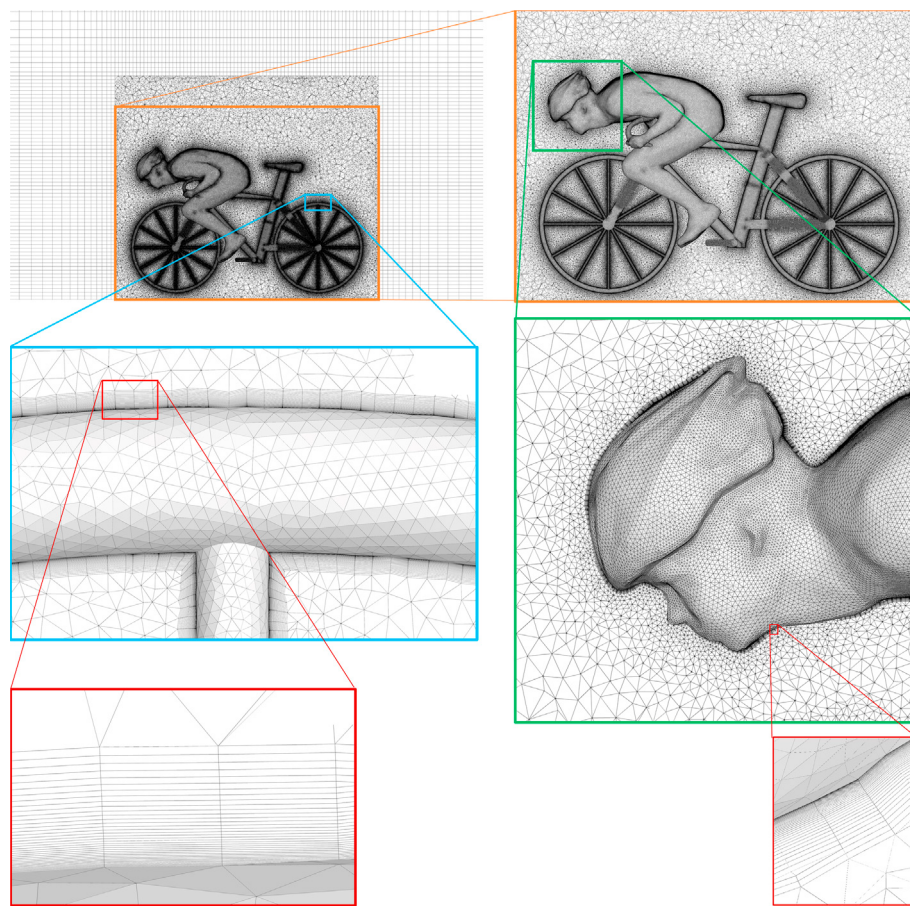


**Fig. 9.** Details of computational grid on cyclist and bicycle surfaces and in the vertical centerplane. Wall-adjacent cell size is 20 micrometer, 40 layers of prismatic cells are used in the boundary layer.

aerodynamic performance (You Tube, 2017). For all fifteen positions, Fig. 14 shows the values of the sagittal torso angle, the shoulder angle, the elbow angle, the forearm angle, the hip angle, the knee angle and the ankle angle.

#### 4.2. Computational settings and parameters

The simulations were performed at full scale. The models were placed in a computational domain with size according to best practice guidelines (Franke et al., 2007; Tominaga et al., 2008; Blocken, 2015):  $L \times W \times H = 33.79 \times 16.49 \times 9.73 \text{ m}^3$ . The maximum blockage ratio was 0.2%, which is well below the recommended maximum value of 3% (Franke et al., 2007; Tominaga et al., 2008). The directional blockage ratios were also well below 17% (Blocken, 2015). Given these low blockage ratios, the CFD simulations were not corrected for blockage. The grids were similar to those outlined above (Figs. 8 and 9). The solver settings (approximate form of the governing equations, turbulence model, discretization schemes, etc) were identical to those in section 3.

#### 4.3. Results: drag area and ranking

Fig. 15 ranks the 11 road race positions from lowest to highest drag area. The position “Top tube 4” has the lowest drag area. This position is followed by “Top tube 3”, which has a slightly higher drag area, because of the higher position of the head. The “Pantani” position ranks as number 3. The least aerodynamic positions are the position “Elbows” and the position “Back up”, the latter of which has a drag area that is 38% higher than “Top tube 4”. Fig. 15 also shows, for every position, the percentage that this position is slower compared to the reference position

“Top tube 4”. It is assumed that all cyclists are not pedaling (static legs) and keep the same position throughout the descent. The percentage numbers can be used to determine the additional time needed for a given descent with reference to the fastest position. Let us assume a downhill distance of 5 km with cycling speed 20 m/s (72 km/h) in position “Top tube 4”, then the extra time in seconds needed to complete this descent using other descent positions is given by the numbers in Fig. 15. Considering that races are sometimes won by a few seconds, these time differences can be considered to be very large.

Fig. 16 provides similar information for the time trial positions. While it was expected that the position with regular helmet would be the slowest, it is clearly shown here that sitting on the top tube in a hill descent can yield very large benefits in time trials that include steep hill descents.

#### 4.4. Results: surface static pressure coefficients

The pressure coefficient  $C_p$  is defined as:

$$C_p = 2 \frac{P - P_0}{\rho U_\infty^2} \quad (2)$$

where  $P$  is the static pressure and  $P_0$  the reference static pressure (= atmospheric pressure).

Fig. 17 compares the surface pressure coefficients for the five positions with the cyclist sitting on the saddle. The highest frontal area and the highest drag area are found for the “Back up” position, the lowest frontal area and the lowest drag area are found for the position “Back down 2”. Fig. 17a shows larger areas on the cyclist back with low  $C_p$  (blue color), while Fig. 17d shows the least area with low  $C_p$ . Also, Fig. 17c and

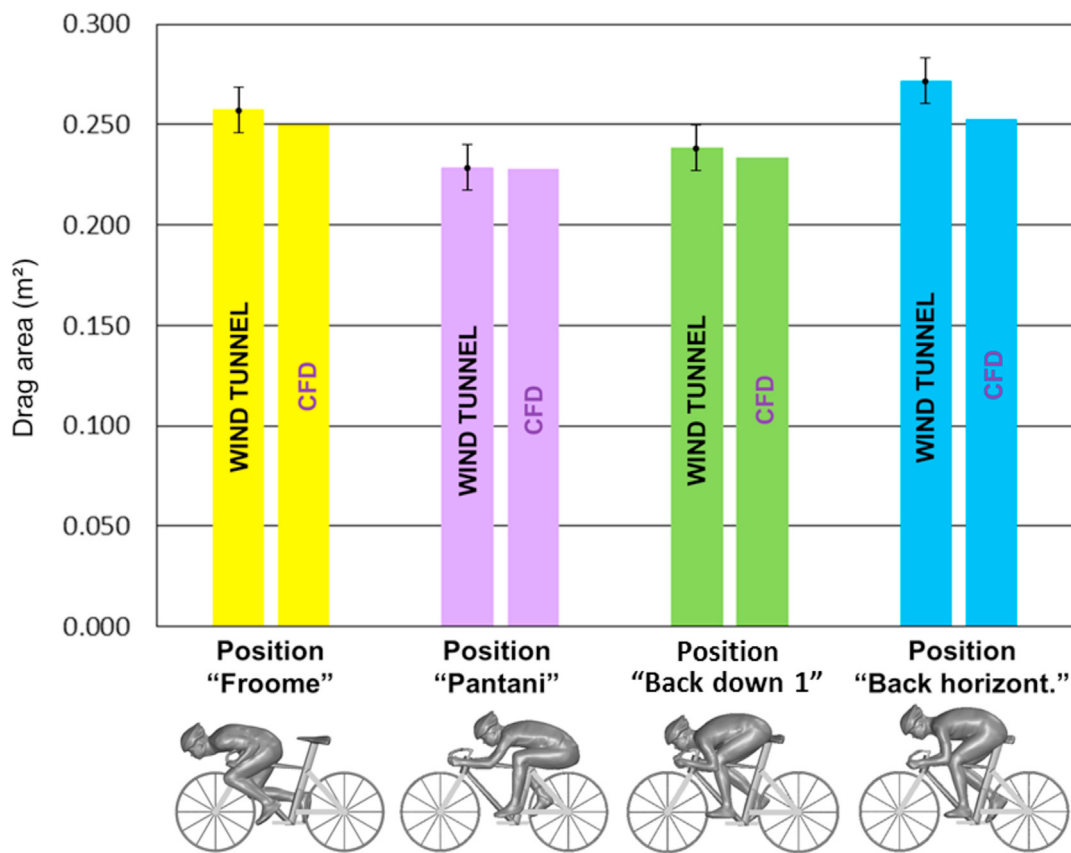


Fig. 10. Comparison of wind tunnel and CFD results for the four tested models in terms of drag area.

d shows the smallest areas with large  $C_p$  (red color) on the front part of the cyclist. Note that suction on the lateral sides of the cyclist does not contribute to cyclist drag. This figure suggests a complex flow pattern with multiple separation and reattachment areas.

Fig. 18 provides the surface pressure coefficients for the five positions with the cyclist sitting on the top tube. The highest frontal area and the highest drag area are found for the "Top tube 1" position, while the lowest frontal area and the lowest drag area are found for the "Top tube 4" position. One might assume that a higher frontal area would yield a higher drag area. This appears to be generally the case, except for the "Froome" position that has a lower frontal area than the "Top tube 2 and 3" positions, but a higher drag area than these positions. For the "Froome" position, the areas with large (positive – red/yellow color)  $C_p$  on the shoulders and also on the upper legs are larger than the "Top tube 2" position. And although the  $C_p$  on the cyclist's back is on average less negative (less suction) in the "Froome" position than in the "Top tube 2" position, the areas with lowest  $C_p$  on the back of the "Top tube 2" position are located near the shoulders on surfaces that are nearly horizontal, so they do not contribute substantially to the drag. For the "Froome" position, the areas with lowest  $C_p$  on the back of the cyclist are situated at the sides of the lower back on surfaces that are inclined and do yield a force component in the streamwise direction. While Fig. 18e shows substantial areas of low (negative)  $C_p$  on the cyclists shoulders, also these areas are almost horizontal and do not contribute substantially to the drag area.

Fig. 19 shows the surface pressure coefficients for the five remaining positions. The highest frontal area and the highest drag area are obtained for the "Time trial with regular helmet" position, while the lowest frontal area and the lowest drag area – as expected – are obtained for the "Superman" position. Fig. 19c shows that the areas of low  $C_p$  on the cyclist back are more pronounced. However, the areas near the shoulders are nearly horizontal while the areas at the lower back do contribution to the suction exerted on the rider. However, this effect appears to be

compensated by the lower frontal area and therefore smaller areas with high  $C_p$ .

#### 4.5. Results: frontal area, form drag and friction drag

Some additional results are provided in Figs. 20–22.

Fig. 20 shows the ratio of the drag area only by form drag to the total drag area (form drag + friction drag) as a function of the total drag area for all 15 cyclist positions. It indicates that in the present study, the form drag constitutes about 94–97% of the total drag. It should be noted here that smooth cyclist and bicycle surfaces were adopted for the CFD simulations. In reality, the roughness of the cyclist body and clothing, especially when wearing skinsuits, will cause the friction drag to increase in absolute terms while the form drag might decrease in absolute terms. Both changes will cause the ratio of from drag to total drag to decrease. Unsurprisingly, the highest percentage of form drag is provided by the "Back up" position, while the lowest percentage is obtained by the "Superman" position. However, there is not a monotonic increase of the percentage of form drag with increasing  $C_dA$ .

Fig. 21 illustrates the frontal area versus the drag area. The highest and lowest drag areas are associated with the "Back up" and "Superman" positions, and these also yield the highest and lowest drag areas, respectively. Also here, there is not a monotonic increase of the drag area with increasing  $C_dA$ , or, conversely, the drag area does not increase monotonically with increasing A. This is related to the values of the drag coefficients that are largely determined by the location of the flow separation points and reattachment points on the body of the cyclist and on the bicycle and by the pressure action in the areas of separated flow. Figs. 17–19 indicated that the separation areas (i.e. the dark blue areas) have clearly different locations for the different cyclist positions. Table 1 provides the overview of the drag coefficients of all positions together with the A and  $C_dA$  values.

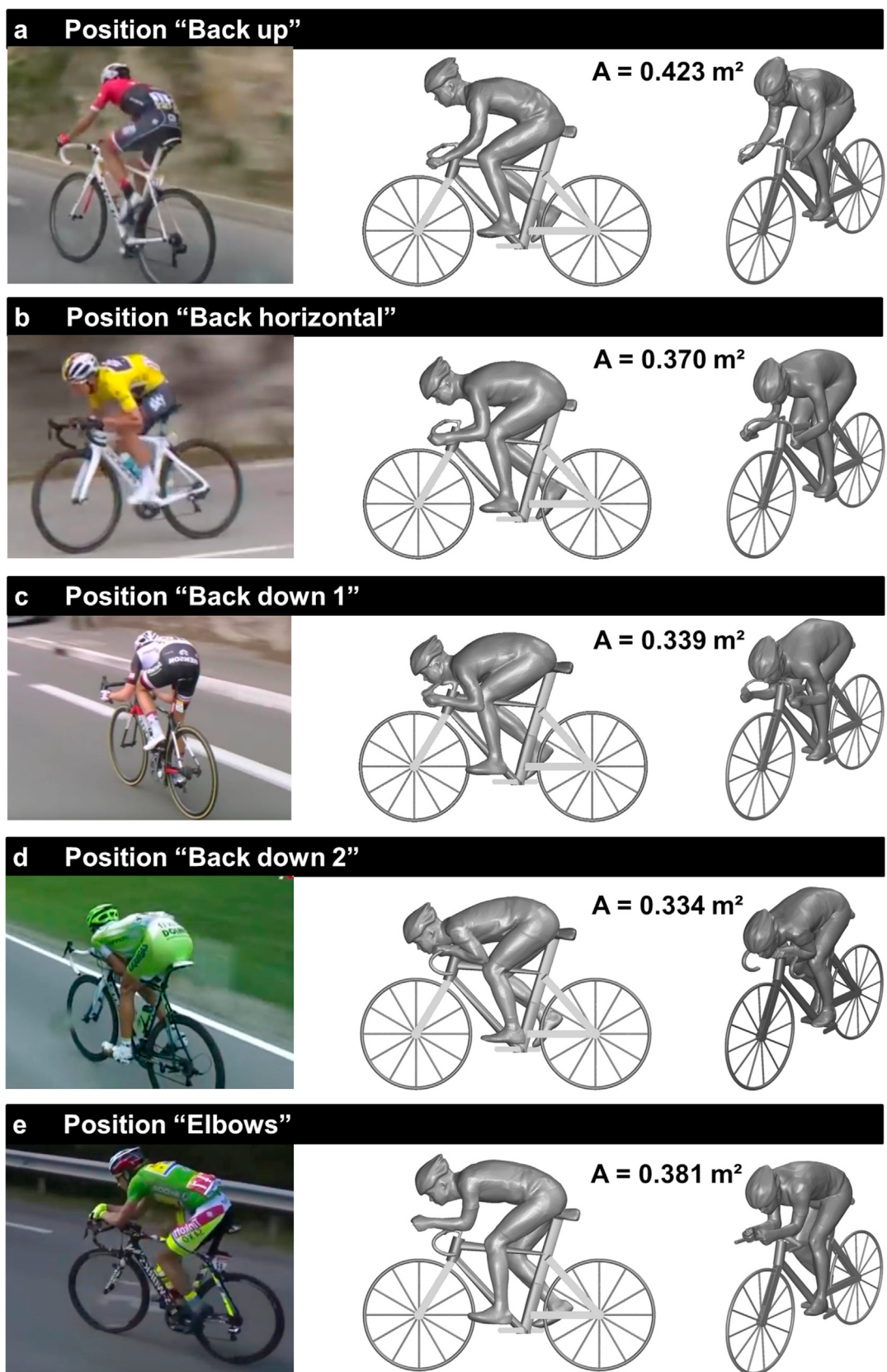


Fig. 11. Photographs, side views and perspective views of first set of five positions, all with cyclist sitting on saddle. Frontal area is indicated.

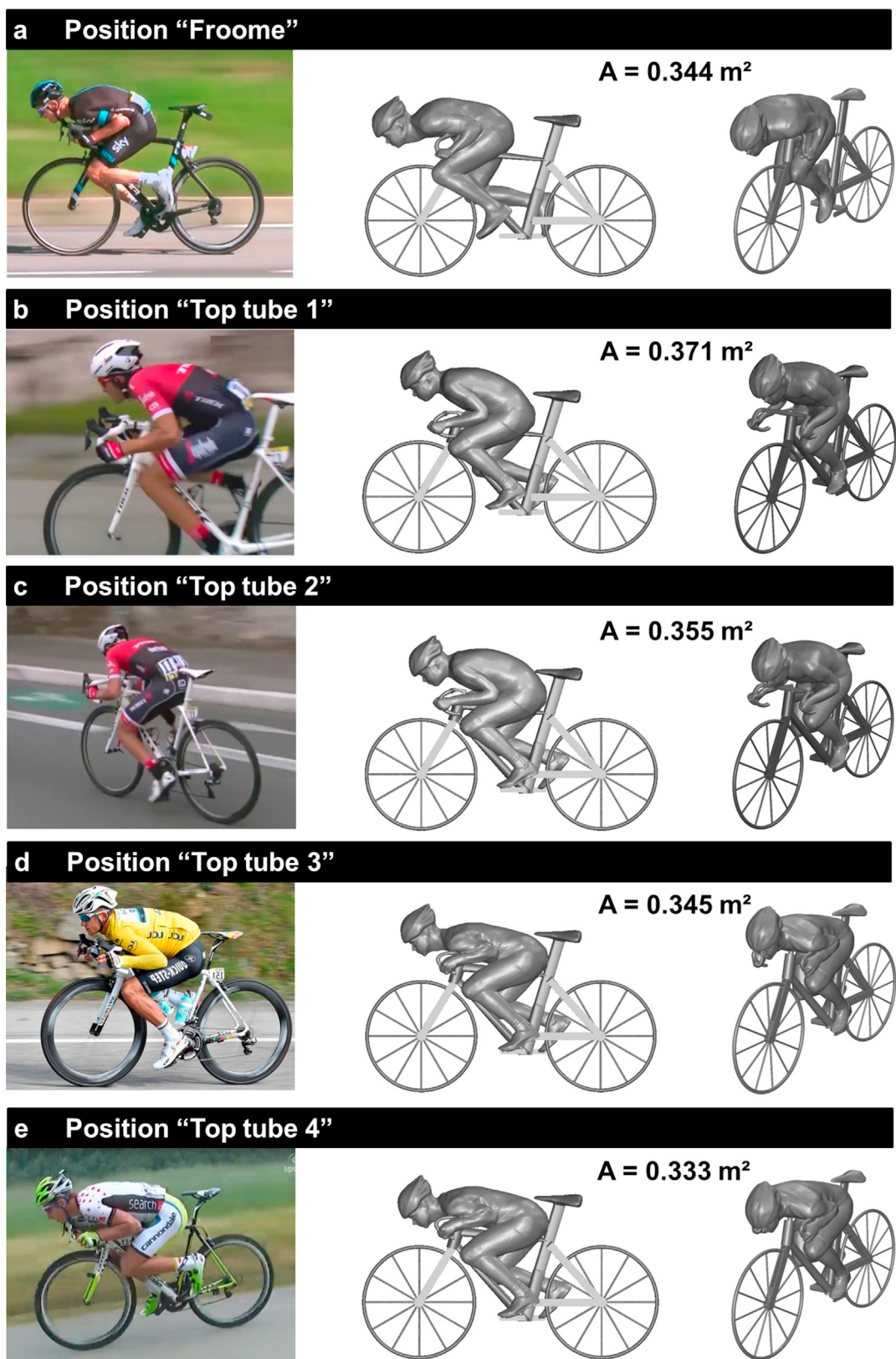


Fig. 12. Photographs, side views and perspective views of second set of five positions, all with cyclist sitting on top tube. Frontal area is indicated.

Fig. 22 provides two nomograms that indicate the extra time required in seconds, per km and compared to the fastest descent position, as a function of the cycling speed  $U$  and with the position as a parameter. These nomograms allow estimating the time gain (or time lost) by a given position compared to those fastest positions.

## 5. Discussion

The study assumed that the hill slope is steep and straight enough so that pedaling to gain speed and changes in positions for sharp bends are not needed. These conditions were representative of part of the

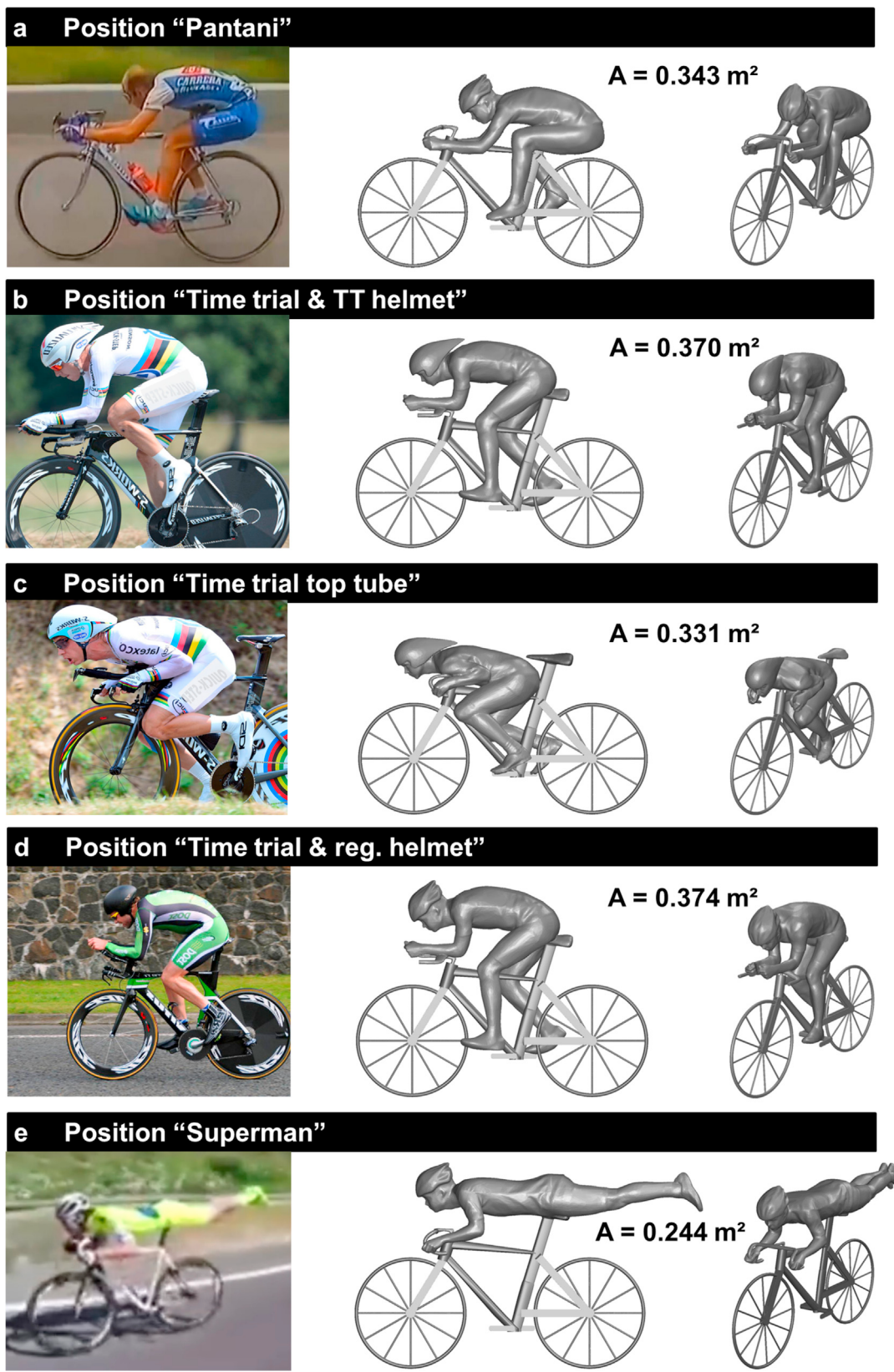
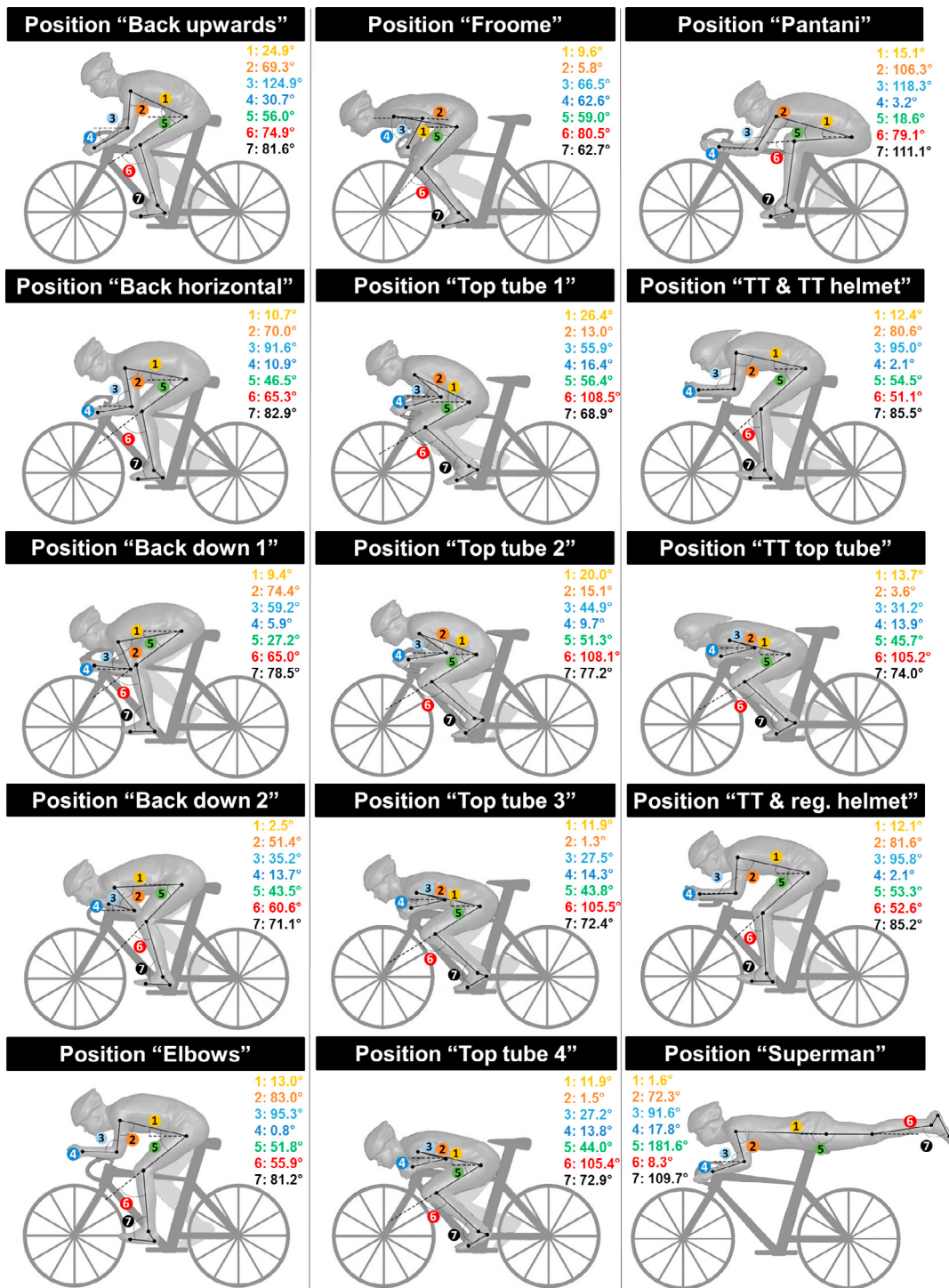


Fig. 13. Photographs, side views and perspective views of third set of five positions. Frontal area is indicated.

Peyresourde descent. However, for many other hill descents, pedaling will be needed and/or a more equal distribution of the cyclist body weight over the two wheels will be needed for better stability and steering capacity in sharp bends. Returning to Fig. 15, the positions that

allow pedaling (from fastest to slowest) are “Top tube 2”, “Back down 1”, “Froome”, “Back horizontal”, “Top tube 1”, “Elbows” and “Back up”. However, pedaling in positions such as “Top tube 2”, “Back down 1”, “Froome” and “Top tube 1” will be more difficult as in positions such as



**Fig. 14.** The fifteen cyclist positions with values of (1) sagittal torso angle; (2) shoulder angle; (3) elbow angle; (4) forearm angle; (5) hip angle; (6) knee angle; (7) ankle angle.

"Back horizontal", "Elbows" and "Back up". Concerning steering capability in sharp bends, it is expected that this will not be hampered only for positions "Back down 1", "Back horizontal" and "Back up". If the requirements of pedaling at high power output and full steering capability are combined, if a single best overall position has to be selected, this would be "Back down 1" or "Back horizontal". For optimal performance in a descent where pedaling and steering capability are required, it might be best to combine different positions, e.g. to alternate "Top tube 4" for the steep parts where no pedaling and steering are required, and "Back down 1" or "Back horizontal" for the parts where either pedaling or

steering are needed. However, it is possible that alternating between different positions is only really worthwhile when this alternating action would not occur too frequently, as it can be expected that additional aerodynamic losses occur by the action of moving from one position to another.

Although this study was based on detailed and validated CFD simulations applied for a wide range of cyclist hill descent positions, there are also some limitations related to the choice of cyclist model. The cyclist positions were all based on scans of the same person with given body characteristics. This was done to allow a clear comparison between the

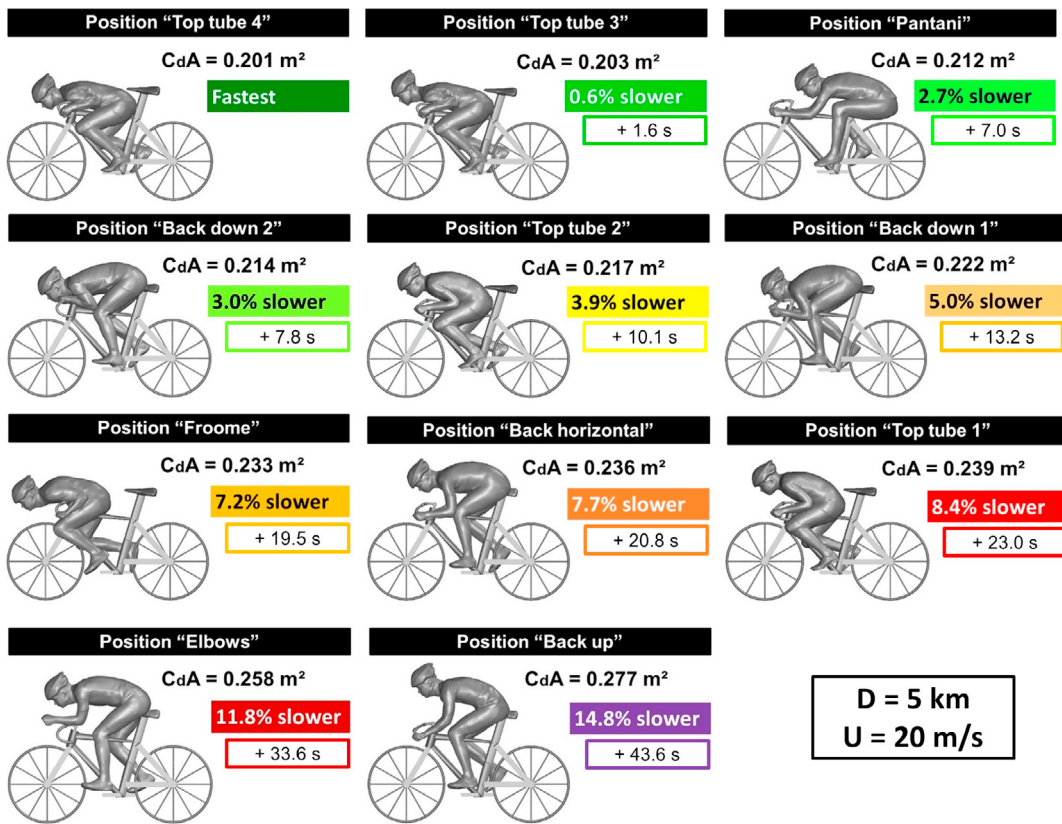


Fig. 15. Ranking of 11 road race positions from fastest to slowest.  $C_dA$  is indicated, as well as percentage of speed decrease and time lost by a given position compared to the fastest one on a 5 km downhill distance at 20 m/s without pedaling.

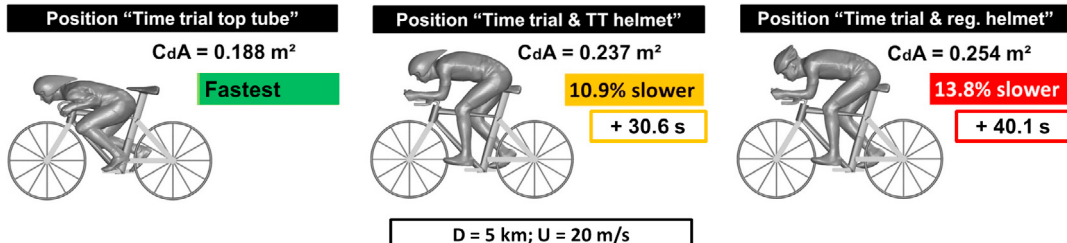


Fig. 16. Ranking of three time trial positions from fastest to slowest.  $C_dA$  is indicated, as well as percentage of speed decrease and time lost by a given position compared to the fastest one on a 5 km downhill distance at 20 m/s without pedaling.

different positions and to remove anthropometric bias. Although the values of the frontal area, drag coefficient and drag area will differ for different athletes, it is expected that the main trends found in the present study will be similar for different athletes, although the precise numbers will undoubtedly vary. It is expected that the largest deviations from the present study will occur for cyclists that are at the extremes of the anthropometric spectrum, i.e. very tall or very short athletes, or athletes with very large or small leg/torso ratio. Therefore, future research should focus on the aerodynamic performance of hill descent position of these athletes as well.

The CFD simulations and the wind tunnel measurements in the present paper had static legs and the wheels were fixed. Earlier research has shown that the aerodynamic drag of a pedaling cyclist, averaged over one pedaling revolution, is quite similar to that of the same cyclist with the crank almost horizontal (Crouch et al., 2016). An indication of the effect of rotating wheels was provided by Blocken et al. (2018) where it was shown that for the cyclist in "Back up" position, the CFD simulation for the static wheels yielded a drag force of 36.06 N, while the simulation for the same geometry with rotating wheels yielded 37.30 N. This would

indicate that wheel rotation is not a major factor in the aerodynamic drag of an isolated cyclist, at least in the absence of cross wind.

All CFD simulations and wind tunnel measurements in this study assumed that the cyclist(s) was/were riding in still air, so no head wind, tail wind or cross wind is present. Future research should investigate especially the effect of cross wind on the drag area of different cyclist hill descent positions. Other simplifications in this study included the steady-state calculations (in spite of the pseudo-transient approach) and the assumption that the cyclist surfaces were smooth; so no special skinsuits with roughness texture were included. The use of such skinsuits can further reduce the drag areas.

Given the evidence presented in this paper that the "Froome" position is not aerodynamically superior to many other cycling hill descent positions, the question remains why top athlete Chris Froome won stage 8 in the 2016 Tour de France. This was due to the combination of the following reasons. First, he already accelerated and broke away before reaching the top of the Peyrejourde, and started the descent while the chasers were still climbing. When one starts descending at high speed while others are still climbing, already a substantial lead is established.

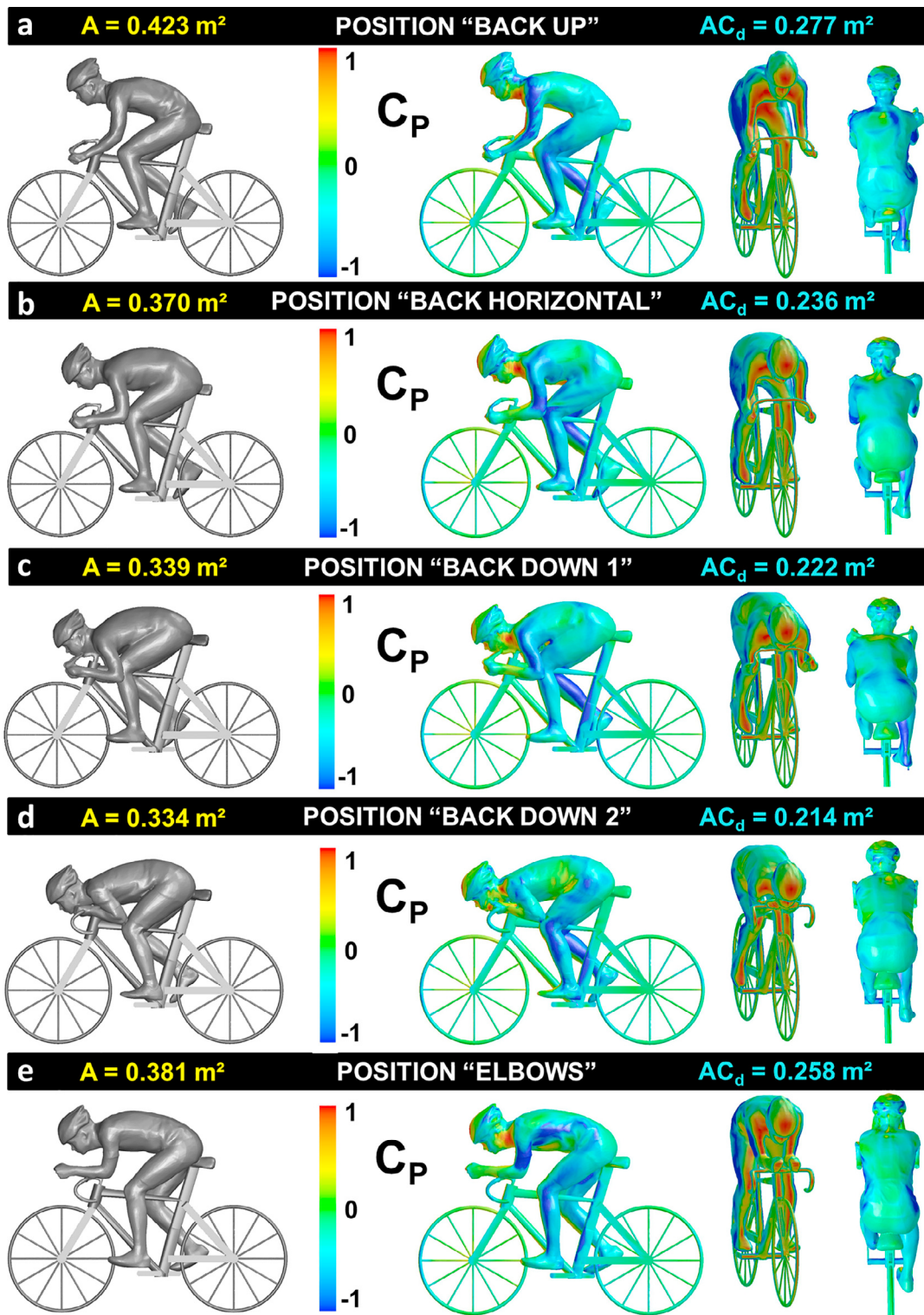
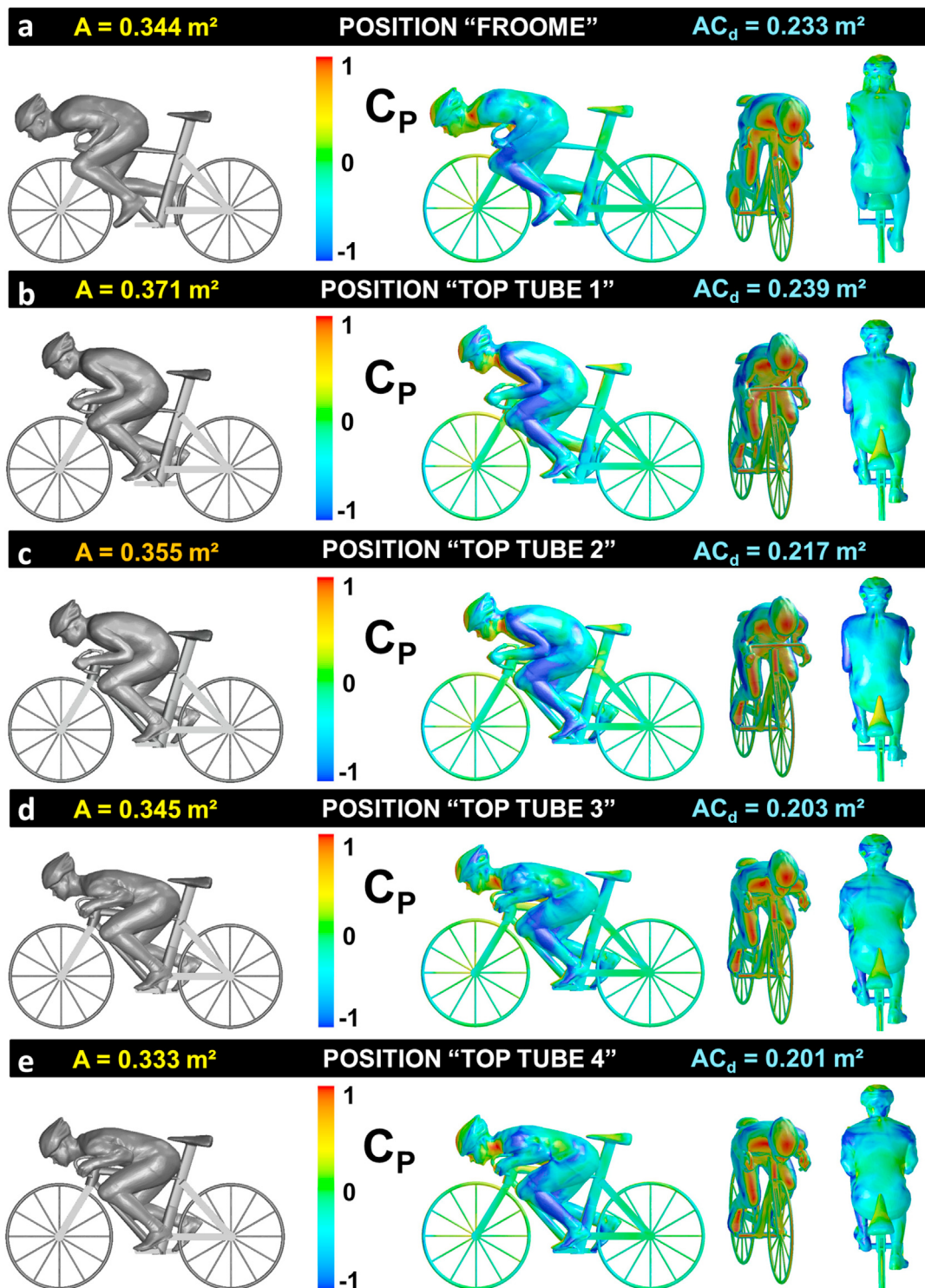


Fig. 17. Static pressure coefficient on cyclist and bicycle surfaces for the first set of five positions (cyclist on saddle). Frontal area and drag area are also indicated.

Second, when he broke away, the chasers initially hesitated for quite a while, looked over their back to see who would lead the chase, and while doing this they were riding slowly in "Back up" position. It is clear from the present study that the "Back up" position is substantially aerodynamically inferior to the "Froome" position. Third, also during later parts of the descent, the chasers assumed the "Back up" or the "Back horizontal" position, both of which are slower than the "Froome" position (see Fig. 15).

## 6. Conclusions

Different professional cyclists were using very different hill descent positions, which indicated that prior to the present study, which was first communicated via a LinkedIn article on 28 April 2017, there was no consensus on which position is really superior, and that most cyclists did not test different positions, for example in wind tunnels, to find which position would give them the largest advantage. This paper presented an



**Fig. 18.** Static pressure coefficient on cyclist and bicycle surfaces for the second set of five positions (cyclist on top tube). Frontal area and drag area are also indicated.

aerodynamic analysis of 15 different hill descent positions. It was assumed that the hill slope was steep enough so pedaling was not required to gain speed and that the descent did not include sharp bends necessitating changes in position. Cross wind was not considered. All simulations and wind tunnel tests were made for cyclist positions obtained by 3D scanning of the same athlete to remove anthropometric bias. Under these assumptions and for the given athlete basic anthropometry, the following conclusions were obtained:

- The fastest road race position analyzed is “Top tube 4”, where the cyclist sits on the rear part of the top tube with torso stretched towards the steering wheel and the head sufficiently down.
- The slowest road race position analyzed is “Back up”, where the cyclist sits on the saddle with the back directed upwards and the head also upright.
- The infamous “Froome” position is not aerodynamically superior to several other positions. It is 7.2% slower than the “Top tube 4”

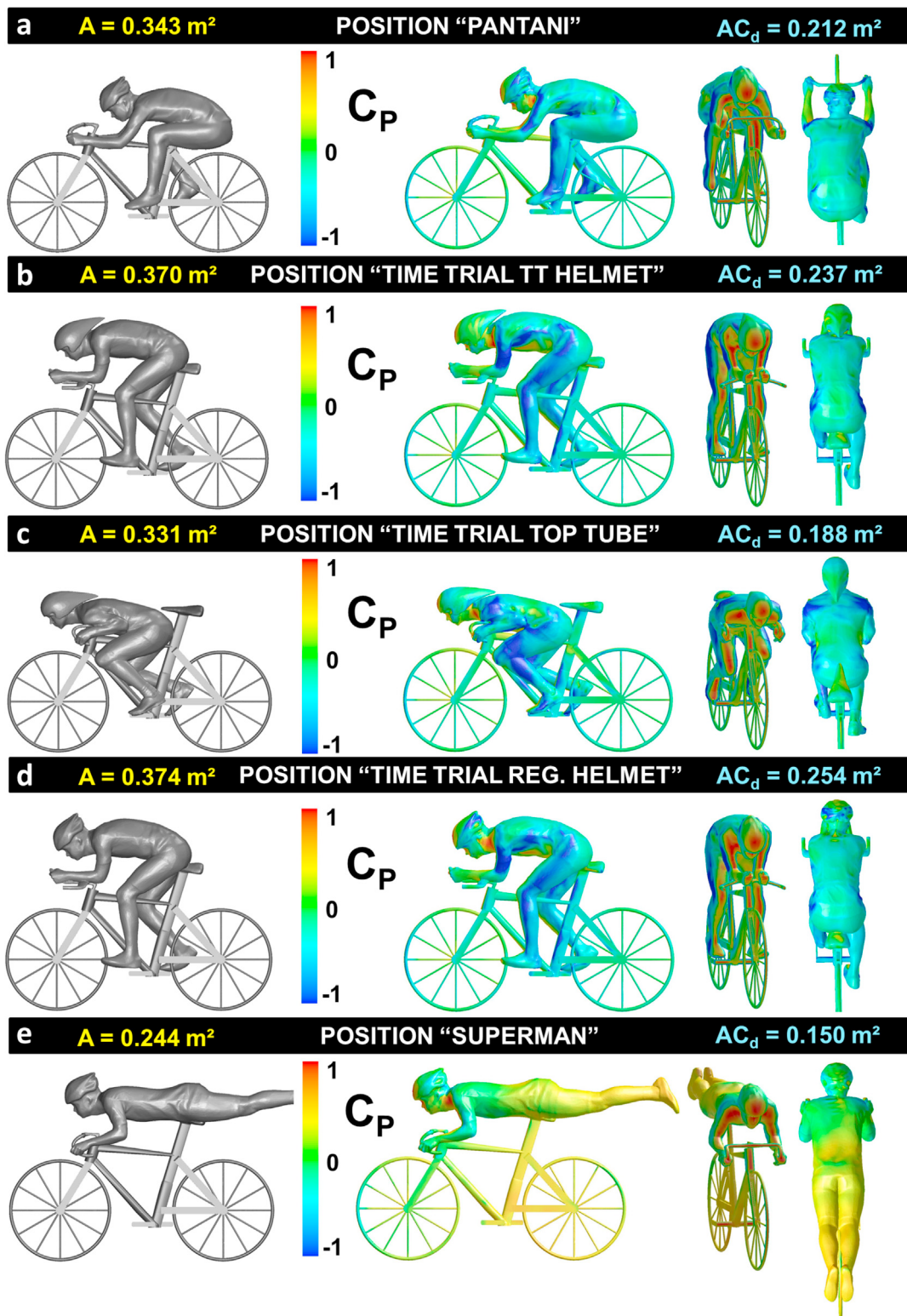


**Fig. 19.** Static pressure coefficient on cyclist and bicycle surfaces for the third set of five positions. Frontal area and drag area are also indicated.

position. Of the 11 road race positions analyzed, there are 6 positions that are clearly aerodynamically superior than the “Froome” position. • The fastest time trial (TT) position analyzed is the one on the top tube, which is 10.9% faster than the regular TT position where the cyclist seated on the saddle. • The drag consists for 94 up to more than 97% of form drag. This is partly due to the assumption of smooth cyclist and bicycle surfaces, but it also suggests that the aerodynamic performance of the current

“smooth” cyclist configurations can be substantially further improved by the adoption of skinsuits with specific roughness patches at the positions where flow separation is expected to occur.

- There is not a monotonic increase of the drag area with increasing frontal area. This means that the frontal area should not be used as an indicator of the aerodynamic performance of a given position – although this is often done in practice.

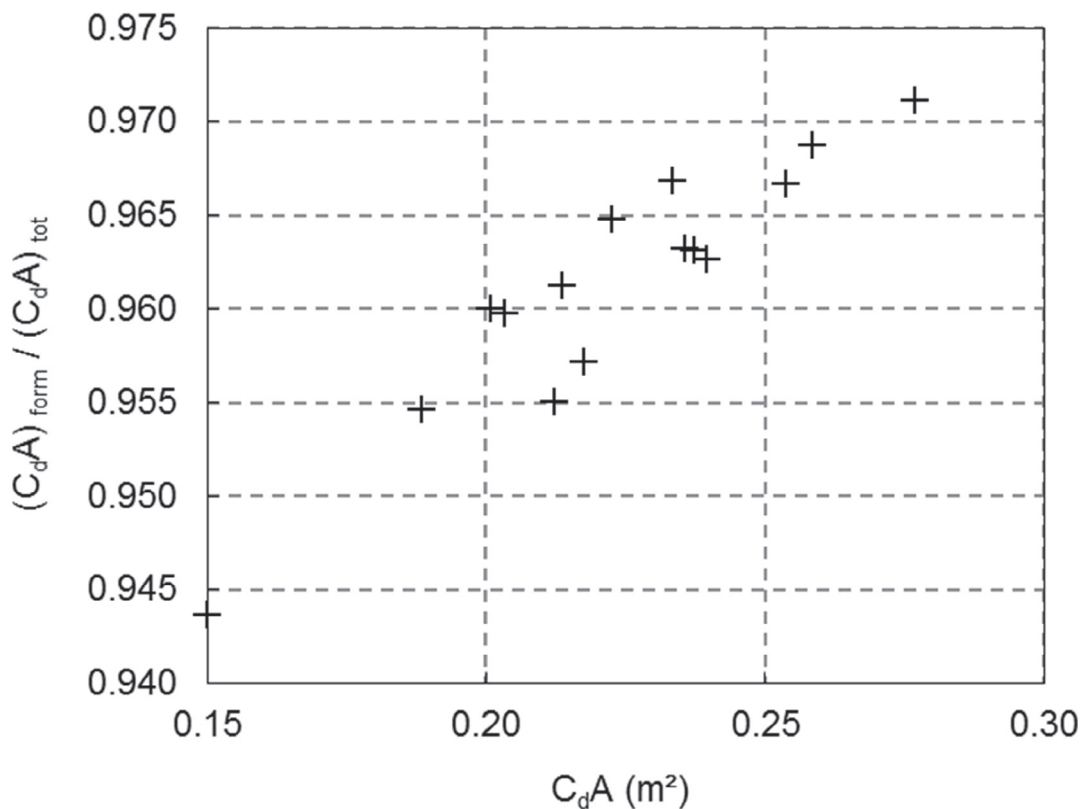


Fig. 20. Ratio of drag area by form drag to total drag area as a function of the total drag area, for all 15 cyclist positions.

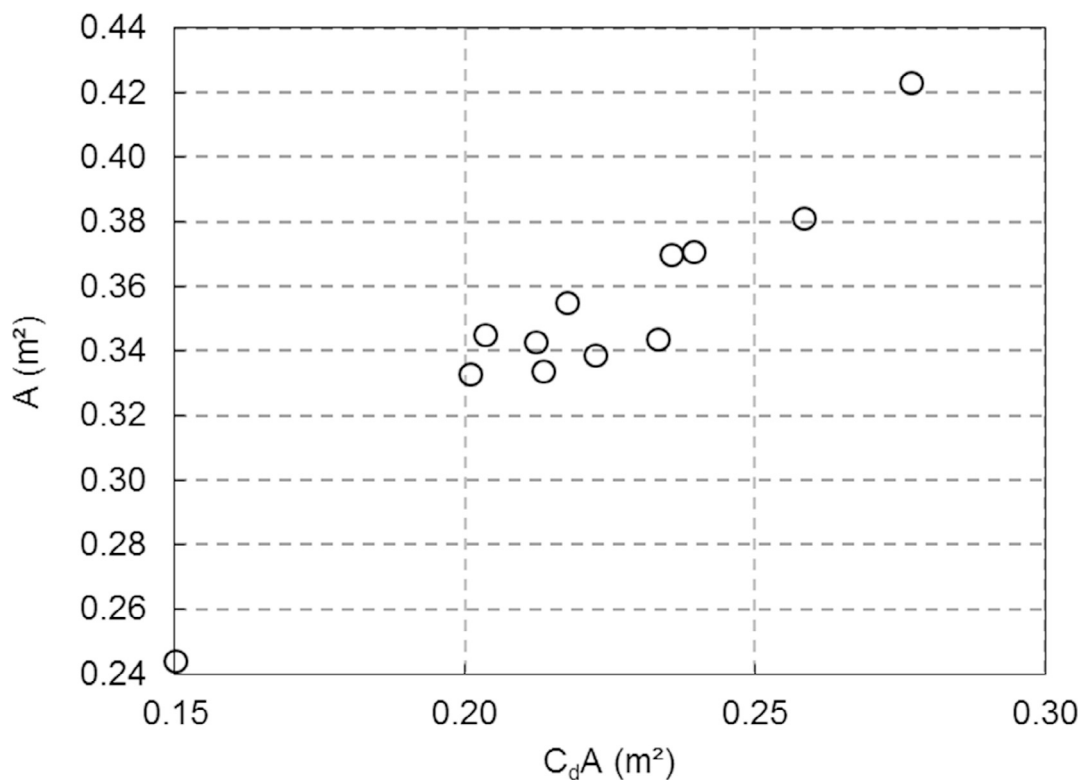
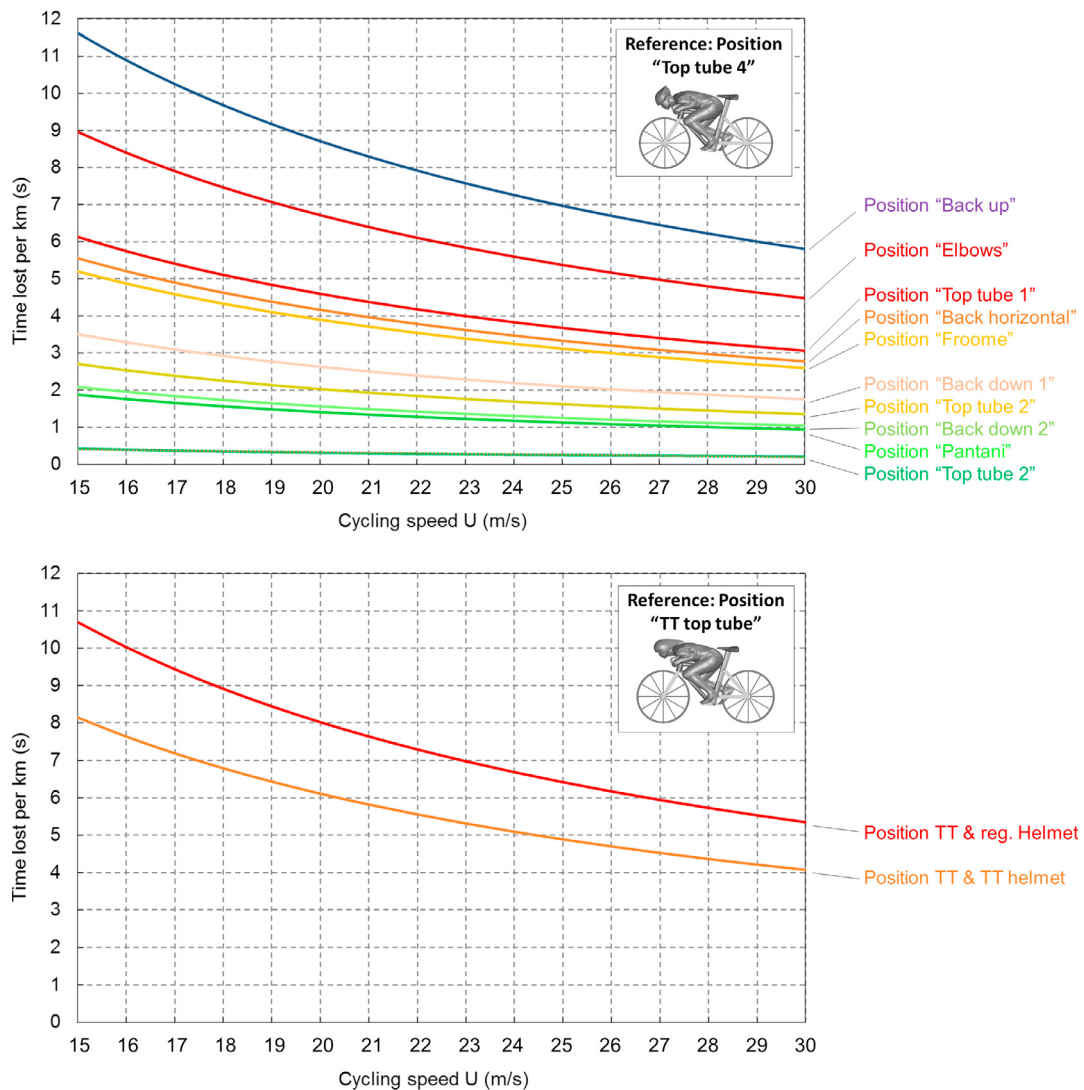


Fig. 21. Frontal area versus drag area, for all 15 cyclist positions.



**Fig. 22.** Nomograms indicating the time lost per km relative to the fastest position (“Top Tube 4” for road race or “Time trial top tube” for time trial), as a function of cycling speed. Parameter in the graphs is the cyclist position. Top: road race positions. Bottom: time trial positions.

**Table 1**  
Frontal area, drag coefficient and drag area for the 15 cyclist positions.

Position	A ( $\text{m}^2$ )	$C_d$ (-)	$C_d A$ ( $\text{m}^2$ )
Back up	0.423	0.655	0.277
Back horizontal	0.370	0.638	0.236
Back down 1	0.339	0.655	0.222
Back down 2	0.334	0.641	0.214
Elbows	0.381	0.677	0.258
Froome	0.344	0.677	0.233
Top tube 1	0.371	0.644	0.239
Top tube 2	0.355	0.611	0.217
Top tube 3	0.345	0.588	0.203
Top tube 4	0.333	0.604	0.201
Pantani	0.343	0.618	0.212
Time trial & TT helmet	0.370	0.641	0.237
Time trial top tube	0.331	0.568	0.188
Time trial & reg. Helmet	0.374	0.679	0.254
Superman	0.244	0.615	0.150

In many descents, the ability to provide large power output and steering capability will also be important. Also in those cases, the “Froome” position is not considered the best. Other positions such as “Back down 1” have a lower drag area, allow better pedaling and are safer because they provide more equal distribution of body weight over both wheels. An

optimal descent might be achieved by combining several positions, e.g. “Top tube 4” for the steep parts where no pedaling and steering are required, and “Back down 1” or “Back horizontal” for the parts where either pedaling or steering are needed.

#### Acknowledgements

An important task of universities nowadays is to communicate their findings to the public. In that respect, the present authors have found an unexpected but very welcome ally in current threefold Road Cycling World Champion Peter Sagan, who picked up this research on social media and who communicated it on 9 May 2017 on Facebook to his hundreds of thousands of followers, stating his interest in this work. We thank Peter and his team for their interest. The authors also thank the technical support team of the Department of the Built Environment at Eindhoven University of Technology, Ing. Jan Diepens, Geert-Jan Maas and Stan van Asten for preparing and setting up the wind tunnel experiments in the wind tunnel laboratory in Liège. The authors also acknowledge the partnership with ANSYS CFD. This work was also sponsored by NWO Exakte en Natuurwetenschappen (Physical Sciences) for the use of supercomputer facilities, with financial support from the Nederlandse Organisatie voor Wetenschappelijk Onderzoek (Netherlands Organization for Scientific Research, NWO). The authors

are most grateful also to the anonymous reviewers for providing many valuable comments that have improved this manuscript.

## References

- ANSYS, Fluent, November 2013. Release 15.0, Theory Guide. ANSYS Inc.
- Artec Europe, 2017. Artec Eva, 3D scanners. Retrieved May 22, 2017, from <https://www.artec3d.com/3d-scanner/artec-eva>.
- Barlow, J.B., Rae, W.H., Pope, A., 1999. Low-speed Wind Tunnel Testing, third ed. Wiley.
- Barry, N., Burton, D., Sheridan, J., Thompson, M., Brown, N.A.T., 2015. Aerodynamic drag interactions between cyclists in a team pursuit. *Sports Eng.* 18 (2), 93–103.
- Beaumont, F., Taiar, R., Polidori, G., Trenchard, H., Grappe, F., 2018. Aerodynamic study of time-trial helmets in cycling racing using CFD analysis. *J. Biomech.* 67, 1–8.
- Blocken, B., Defraeye, T., Koninckx, E., Carmeliet, J., Hespel, P., 2013. CFD simulations of the aerodynamic drag of two drafting cyclists. *Comput. Fluids* 71, 435–445.
- Blocken, B., 2014. 50 years of computational wind engineering: past, present and future. *J. Wind Eng. Ind. Aerod.* 129, 69–102.
- Blocken, B., Toparlar, Y., 2015. A following car influences cyclist drag: CFD simulations and wind tunnel measurements. *J. Wind Eng. Ind. Aerod.* 145, 178–186.
- Blocken, B., 2015. Computational Fluid Dynamics for Urban Physics: importance, scales, possibilities, limitations and ten tips and tricks towards accurate and reliable simulations. *Build. Environ.* 91, 219–245.
- Blocken, B., Toparlar, Y., Andrianne, T., 2016. Aerodynamic benefit for a cyclist by a following motorcycle. *J. Wind Eng. Ind. Aerod.* 155, 1–10.
- Blocken, B., van Druenen, T., Toparlar, Y., Malizia, F., Mannion, P., Andrianne, T., Marchal, T., Maas, G.J., Diepens, J., 2018. Aerodynamic drag in cycling pelotons: new insights by CFD simulation and wind tunnel testing. *J. Wind Eng. Ind. Aerod.* 179, 319–337.
- Casey, M., Wintergerste, T., 2000. Best Practice Guidelines. ERCOFATC Special Interest Group on "Quality and Trust in Industrial CFD", ERCOFATC.
- Crouch, T.N., Burton, D., Brown, N.A.T., Thomson, M.C., Sheridan, J., 2014. Flow topology in the wake of a cyclist and its effect on aerodynamic drag. *J. Fluid Mech.* 748, 5–35.
- Crouch, T.N., Burton, D., Thompson, M.C., Brown, N.A.T., Sheridan, J., 2016. Dynamic leg-motion and its effect on the aerodynamic performance of cyclists. *J. Fluid Struct.* 65, 121–137.
- Crouch, T.N., Burton, D., LaBry, Z.A., Blair, K.B., 2017. Riding against the wind: a review of competition cycling aerodynamics. *Sports Eng.* 20 (2), 81–110.
- Dal Monte, A., Leonardi, L.M., Menchinelli, C., Marini, C., 1987. A new bicycle design based on biomechanics and advanced technology. *Int. J. Sport Biomedech.* 3, 287–292.
- Defraeye, T., Blocken, B., Koninckx, E., Hespel, P., Carmeliet, J., 2010a. Aerodynamic study of different cyclist positions: CFD analysis and full-scale wind-tunnel tests. *J. Biomech.* 43 (7), 1262–1268.
- Defraeye, T., Blocken, B., Koninckx, E., Hespel, P., Carmeliet, J., 2010b. Computational Fluid Dynamics analysis of cyclist aerodynamics: performance of different turbulence-modelling and boundary-layer modelling approaches. *J. Biomech.* 43 (12), 2281–2287.
- Defraeye, T., Blocken, B., Koninckx, E., Hespel, P., Carmeliet, J., 2011. Computational fluid dynamics analysis of drag and convective heat transfer of individual body segments for different cyclist positions. *J. Biomech.* 44 (9), 1695–1701.
- Defraeye, T., Blocken, B., Koninckx, E., Hespel, P., Verbogen, P., Nicolai, B., Carmeliet, J., 2014. Cyclist drag in team pursuit: influence of cyclist sequence, stature, and arm spacing. *J. Biomech. Eng.-ASME* 136 (1) art. no. 011005.
- Fintelman, D.M., Sterling, M., Hemida, H., Li, F.X., 2014a. The effect of crosswinds on cyclists: an experimental study. *The Engineering of Sport 10. Procedia Eng.* 72, 720–725.
- Fintelman, D.M., Sterling, M., Hemida, H., Li, F.X., 2014b. Optimal cycling time trial position models: aerodynamics versus power output and metabolic energy. *J. Biomech.* 47 (8), 1894–1898.
- Fintelman, D.M., Hemida, H., Sterling, M., Li, F.X., 2015a. CFD simulations of the flow around a cyclist subjected to crosswinds. *J. Wind Eng. Aerodyn.* 144, 31–41.
- Fintelman, D.M., Hemida, H., Sterling, M., Li, F.X., 2015b. The effect of time trial cycling position on physiological and aerodynamic variables. *J. Sports Sci.* 33 (16), 1730–1737.
- Fintelman, D.M., Sterling, M., Hemida, H., Li, F.X., 2016. Effect of different aerodynamic time trial cycling positions on muscle activation and crank torque. *Scand. J. Med. Sci. Sports* 26 (5), 528–534.
- Franke, J., Hellsten, A., Schlünzen, H., Carissimo, B., 2007. Best Practice Guideline for the CFD Simulation of Flows in the Urban Environment, COST Action 732: Quality Assurance and Improvement of Microscale Meteorological Models, Hamburg, Germany.
- Gore, M., 2016. Personal Communication with Sensor Manufacturer.
- Grappe, G., Candau, R., Belli, A., Rouillon, J.D., 1997. Aerodynamic drag in field cycling with special reference to the Obree's position. *Ergonomics* 40 (12), 1299–1311.
- Grappe, F., Candau, R., Busso, T., Rouillon, J.D., 1998. Effect of cycling position on ventilator and metabolic variables. *Int. J. Sports Med.* 19, 336–341.
- Griffith, M.D., Crouch, T., Thompson, M.C., Burton, D., Sheridan, J., Brown, N.A.T., 2014. Computational fluid dynamics study of the effect of leg position on cyclist aerodynamic drag. *ASME J. Fluids Eng.* 136 (10), 101105.
- Hanna, R.K., 2002. Can CFD make a performance difference in sport? In: Ujihashi, S., Haake, S.J. (Eds.), The Engineering of Sport 4. Blackwell Science, Oxford, pp. 17–30.
- Jeukendrup, A.E., Martin, J., 2001. Improving cycling performance: how should we spend our time and money. *Sports Med.* 31 (7), 559–569.
- Kyle, C.R., Burke, E.R., 1984. Improving the racing bicycle. *Mech. Eng.* 106 (9), 34–45.
- Langtry, R.B., Menter, F.R., 2009. Correlation-based transition modeling for unstructured parallelized computational fluid dynamics codes. *AIAA J.* 47 (12), 2894–2906.
- Lukes, R.A., Chin, S.B., Haake, S.J., 2005. The understanding and development of cycling aerodynamics. *Sports Eng.* 8, 59–74.
- Lukes, R.A., Hart, J.H., Chin, S.B., Haake, S.J., 2004. The aerodynamics of mountain bicycles: the role of computational fluid dynamics. In: Hubbard, M., Mehta, R.D., Pallis, J.M. (Eds.), The Engineering of Sport 5. International Sports Eng Association, Sheffield.
- Mannion, P., Toparlar, Y., Blocken, B., Hajdukiewicz, M., Andrianne, T., Clifford, E., 2018a. Improving CFD prediction of drag on Paralympic tandem athletes: influence of grid resolution and turbulence model. *Sports Eng.* 21 (2), 123–135.
- Mannion, P., Toparlar, Y., Blocken, B., Clifford, E., Andrianne, T., Hajdukiewicz, M., 2018b. Aerodynamic drag in competitive tandem para-cycling: road race versus time-trial positions. *J. Wind Eng. Ind. Aerod.* 179, 92–101.
- Mannion, P., Toparlar, Y., Blocken, B., Clifford, E., Andrianne, T., Hajdukiewicz, M., 2018c. Analysis of crosswind aerodynamics for competitive handcycling. *J. Wind Eng. Ind. Aerod.* 180, 182–190.
- Menter, F.R., Langtry, R., Volker, S., 2006. Transition modelling for general purpose CFD codes. *Flow, Turbulence and Combustion* 77 (1), 277–303.
- Padilla, S., Mujika, I., Angulo, F., Goirieta, J.J., 2000. Scientific approach to the 1-h cycling world record: a case study. *J. Appl. Physiol.* 89, 1522–1527.
- Tominaga, Y., Mochida, A., Yoshie, R., Kataoka, H., Nozu, T., Yoshikawa, M., Shirasawa, T., 2008. AIJ guidelines for practical applications of CFD to pedestrian wind environment around buildings. *J. Wind Eng. Ind. Aerod.* 96 (10–11), 1749–1761.
- Tucker, P.G., Mosquera, A., 2001. NAFEMS Introduction to Grid and Mesh Generation for CFD. NAFEMS CFD Working Group, R0079, 56 pp.
- Vanmarcke, S., 2017. Vive le vélo, VRT Flemish TV show, 14 July 2017.
- Wilson, D.G., 2004. Bicycling Science, third ed. MIT Press, Cambridge, MA.
- You Tube, 2017. <https://www.youtube.com/watch?v=3Iz7ZMAlaCY>.
- Zdravkovich, M.M., Ashcroft, M.W., Chisholm, S.J., Hicks, N., 1996. Effect of cyclist's posture and vicinity of another cyclist on aerodynamic drag. In: Haake (Ed.), The Engineering of Sport. Balkema, Rotterdam, pp. 21–28.